Ecological Informatics 74 (2023) 101969

Contents lists available at ScienceDirect

Ecological Informatics

journal homepage: www.elsevier.com/locate/ecolinf

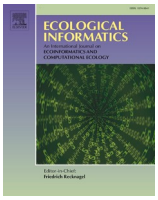

Remote sensing-derived land surface temperature trends over South Asia

Mohamed Shawky [a], M. Razu Ahmed [a], Ebrahim Ghaderpour [a,1], Anil Gupta [a,b], Gopal Achari [a], Ashraf Dewan [c], Quazi K. Hassan [a,*]

[a] Schulich School of Engineering, University of Calgary, 2500 University Drive NW, Calgary, AB T2N 1N4, Canada
[b] Resource Stewardship Division, Alberta Environment and Protected Areas, 3535 Research Road NW, University Research Park, Calgary, AB T2L 2K8, Canada
[c] Spatial Sciences discipline, Curtin University, Bentley 6102, Perth, Western Australia, Australia

ARTICLE INFO

Keywords:
Atmospheric oscillation
Climate change
Cooling trend
Ecoregion
MODIS
Warming trend

ABSTRACT

Spatiotemporal changes in land surface temperature (LST) over South Asia were estimated using MODIS (moderate resolution imaging spectroradiometer) data from 2000 to 2021. We calculated the monthly and annual LST trends and magnitudes by applying the Mann–Kendall test and Sen's slope estimator at both ecoregion and pixel level. More ecoregions experienced daytime cooling than warming. Central and west South Asia showed the highest daytime cooling in December compared to the nighttime warming in the central and northwest in July and September. Nineteen ecoregions demonstrated monthly daytime cooling trends at the 99% confidence level (CL), with the highest record observed in ecoregion *'Indus Valley desert'* in March with the magnitudes of −0.26 °C/yr. While the monthly and annual nighttime warming magnitude was the maximum in *'Gissaro-Alai open woodlands'* in December (0.19 °C/yr at 95% CL), and *'Indus River Delta-Arabian Sea mangroves' at annual scale* (0.06 °C/yr at 99% CL). To understand the influence of large-scale atmospheric oscillations on the trends, we also correlated the estimated LST trends with the selected oscillation indices. Sea surface temperature (SST) Niño 3.4 showed the most significant influence on the trends, where it was positively correlated with 38 ecoregions during nighttime over the year. A better understanding of temperature trends and impacts on South Asia would guide sustainable development and ensures the excessive demands on food, water, and energy supplies coping with the growing population.

1. Introduction

The spatiotemporal variations in temperature (global, regional, and local scales) and related consequences of climate change are threatening human existence, ecological communities, and socioeconomic development across the world (Ahmed et al., 2019b; Di Cecco and Gouhier, 2018; Luintel et al., 2019; Mallick et al., 2022a; Mondal et al., 2014). Over the past decades, the global temperature is mostly increasing at a notable rate (IPCC AR5, 2013), which plunders the living planet Earth by disrupting the normal nature balance and forcing extreme changing weather patterns. Understanding the principal driving factors of warming/cooling trends is the cornerstone for the better implementation of appropriate adaptation and mitigation policies under the temperature changing scenario for a sustainable environment. However, the detailed perception, quantification, and interpretation of the temperature variations, their driving factors, and related consequences have not been done yet for many regions of the world, including the South Asia region. The region consists of eight countries–Afghanistan, Bangladesh, Bhutan, India, Maldives, Nepal, Pakistan, and Sri Lanka, and a living place for about one-fourth (~24%) of the world's population (Babel and Wahi, 2008; The World Bank, 2020) in just ~3.5% of the world's land surface area. The Himalayas, with Mount Everest–the highest mountain in the world, is a major geomorphic landform bordering the north of South Asia that plays a major role in shaping the climate and ecology of the region (Midhuna and Dimri, 2019). It is characterized by snowy peaks and tropical to subtropical climatic conditions at lower and higher altitudes, respectively (You et al., 2017), and controlling the regional weather. The Himalayan glaciers provide the major water supply to the river basins that have experienced volume and mass loss due to the accelerated rate of temperature variations since the mid-twentieth century (Charles, 2008; Nie et al., 2021; Pepin et al., 2015). Also, global warming potentially exerts additional stress on fresh water's need

* Corresponding author.
E-mail address: qhassan@ucalgary.ca (Q.K. Hassan).
[1] Present affiliation: Department of Earth Sciences, Sapienza University of Rome, Piazzale Aldo-Moro, 5, 00185 Rome, Italy.

https://doi.org/10.1016/j.ecoinf.2022.101969
Received 5 November 2022; Received in revised form 24 December 2022; Accepted 26 December 2022
Available online 28 December 2022

for safe drinking and irrigation, particularly with the rising population. Besides, under constant drying conditions in South Asia (Zhai et al., 2020), it becomes a challenge to ensure the supply of food, freshwater, and energy for the world's poor (40%) and food–energy deficient population (51%) (Ahmed et al., 2007). It is crucial, therefore, to evaluate the long- and short-term patterns and magnitudes of temperature variations for sustainable development in the region; although some country-specific studies were found in the literature for Bangladesh (Mallick et al., 2022a), India (Mondal et al., 2014), Nepal (Luintel et al., 2019), and Pakistan (Ahmed et al., 2019b).

Studying the patterns and magnitudes of spatiotemporal changes in temperature are essential to understand the associated climate change consequences. For instance, daily air temperature datasets from 21 circulation models were analyzed between 1871 and 2099 (Di Cecco and Gouhier, 2018) to understand how climatic changes would affect the trends. Also, the Intergovernmental Panel on Climate Change (IPCC) of the United Nations used three gridded global air temperature datasets, i.e., CRU TS 4.04, Berkeley Earth, and HadCRUT5 from CRUTEM5 and HadSST4 (Intergovernmental Panel on Climate Change (IPCC), 2022), for recent past periods to estimate the global warming of 1.5 °C above pre-industrial levels (IPCC, 2018). Weather stations around the globe measure air temperature for the station-point locations that were used for generating these gridded datasets. However, the generation of these datasets is based on the unweighted averaging of the station/location-specific temperature changes (Rahaman et al., 2017). It is because weather stations are densely populated usually in the population centres or agricultural lands and scarce in mountainous or desert areas (Castellanos-Acuna and Hamann, 2020; Menne et al., 2012), and many countries have a very limited number of stations (Gubler et al., 2017). Therefore, it may fail to produce continuous surface temperature dynamics over the non-populated areas of large geomorphic landforms, i.e., mountains and deserts, in the region. Another efficacious alternative is to use land surface temperature (LST) of space-borne remote sensing dataset because of its capacity to provide continuous surface temperature in a finer spatial resolution (e.g., 1 km or better), covering nearly the entire globe. It also have the advantages of repetitive coverage, synoptic view, and near real-time capacities (Ahmed et al., 2019a; Akbar et al., 2019; Tan et al., 2021). It would also be helpful to correlate spatiotemporal dynamics in temperature with any land cover changes (Jiang et al., 2021; Tepanosyan et al., 2021) in South Asia region.

Moderate resolution imaging spectroradiometer (MODIS) onboard Terra/Aqua satellite-derived LST products have been widely employed for local, regional, and global studies in delineating temperature trends since 2000, where both Mann-Kendall and linear regression techniques were commonly used for the time-series analysis (Dewan et al., 2021; Liu et al., 2020; Luintel et al., 2019; NourEldeen et al., 2020; Yan et al., 2020). Processed MODIS LST products are available in three temporal resolutions– daily, 8 days, and monthly with spatial resolutions of 1 km and 0.05° (~5.6 km). These products are analyzed for diurnal (daytime), nighttime, daily, monthly, seasonal, and annual temperature changes. In South Asia, a study on Nepal used the MOD11C3 v006 product of monthly data at a 5.6 Km spatial resolution, and showed an increasing patterns of the nighttime LST (2000–2017) (Luintel et al., 2019). Another study in Bangladesh used MOD11A2 v006 product (8-day/ 1 km) for the 2000–2019 period and reported the annual warming trends were greater in the larger cities than in the smaller cities (Dewan et al., 2021). The MODIS LST datasets have been utilized for similar studies on the globe and other regions/countries since their availability in 2000, such as at the scale of entire world (Liu et al., 2020), North America (Yan et al., 2020), South Africa (NourEldeen et al., 2020), Gongga Mountain in China (Zhao et al., 2021), Tibetan Plateau (Yang et al., 2021), Jordan (Jaber and Abu-Allaban, 2020) and the forests in Aysén region of Chile (Olivares-Contreras et al., 2019).

While the above studies showed mostly the warming trends, some also reported daytime cooling trends (sometimes both warming and cooling) for many countries/regions. For example, Eleftheriou et al. (Eleftheriou et al., 2018) reported the decrease in annual and seasonal trends (2000–2017) in Greece, except winter. Mao et al. (Mao et al., 2017) found daily and seasonal cooling trends in northern regions of China, Mongolia, southern regions of Russia, western regions of Canada and America, eastern and northern regions of Australia, and the southern tip of Africa over the period 2001–2012. Also, Hassan et al. (Hassan et al., 2021) documented daytime cooling in July and August (summer), and November (early winter) for the southern and southeastern natural subregions (sub-ecoregions) of the Alberta province in Canada. The study indicated that ecoregions have a combined influence of climate, topography, and geology due to the variable landscape patterns (land cover), vegetation, soil types, and physiographic features, thus influence the LST trends. Therefore, it might be possible that some ecoregions in South Asia would show cooling trends due to the land cover dynamics and influences of large-scale atmospheric oscillations, in contrast to the global warming trend.

Atmospheric oscillations were shown in the literature as an influential factor of temperature changes in south Asian countries (Iqbal et al., 2016; Islam et al., 2021; Mallick et al., 2022b). In Bangladesh, warming trends were found significantly associated with Atlantic Multidecadal Oscillation (AMO), Arctic Oscillation (AO), East Asian Summer Monsoon Index (EASMI), Sunspot, and South Asian Summer Monsoon Index (SASMI), and cooling trends were linked with AMO for the period 1980–2017 (Islam et al., 2021). Another study showed a significant connection with multivariate ENSO (El Niño-Southern Oscillation) index (MEI), Sea Surface Temperature (SST), Southern Oscillation Index (SOI) and Indian Ocean Dipole (IOD) during the same period (Mallick et al., 2022b). A correlation analysis study in Pakistan was also carried out to depict the relationships of the maximum and minimum temperatures between 1952 and 2009 with oscillation indices (Iqbal et al., 2016). The highest correlations were reported in the pre-monsoon months, i.e., from January to March with North Atlantic Oscillation (NAO) and May with ENSO, and the late pre-monsoon month May with North Sea Caspian (NCP) index. The lowest correlation coefficients were observed with the AO pattern (Iqbal et al., 2016). Other studies were also conducted on Bangladesh, India, and Nepal in finding the relationships of atmospheric oscillations (ENSO, PDO—Pacific Decadal Oscillation, AO, and SST-Nino3.4) with drought events (Azad and Rajeevan, 2016; Shahfahad Talukdar et al., 2022; Sharma et al., 2021; Wang et al., 2013)— mainly a function of variations in precipitation and temperature; and precipitation (Azad and Rajeevan, 2016; Krishnamurthy and Krishnamurthy, 2013; Wahiduzzaman, 2012)— controls the temperature variations. While studies showed having the influences of atmospheric oscillations on temperature variations in some countries of South Asia, we did not find any similar study for the region as a whole.

In this research, the main aim was to study the spatiotemporal variations of LST acquired from MODIS over the South Asia region from 2000 to 2021, and its associated potential driving factors. It can contribute to a better understanding of temperature impacts on South Asia for a sustainable development to ensure the excessive demands to food, water (drinking and irrigation), and energy supplies with the tremendous growth of population. In this context, the detailed objectives were to: (i) estimate the magnitudes and trends of monthly and annual day and nighttime LST time-series over South Asia applying the Mann–Kendall test and Sen's slope estimator, both object- (ecoregion) and pixel-based; and (ii) correlate the estimated LST trends with the selected indices of large-scale atmosphere oscillations, such as ENSO (includes SST - Niño 3.4, SOI, and OLR—outgoing longwave radiation), Dipole Mode Index (DMI), PDO, AO, and North Atlantic Oscillation Index (NAO), to determine any potential influence of atmospheric circulations on the temperature trends in South Asia.

2. Materials and methods

2.1. Study area description

The region South Asia was our study area, which is defined in many ways by multiple global organizations. We adopted the definitions of United Nations and World Bank of comprising eight countries— Afghanistan, Bangladesh, Bhutan, India, Nepal, Maldives, Pakistan, and Sri Lanka. It is located between 5° and 37° in the northern hemisphere with diverse geomorphic and geologic features (Sharma, 2012), including a mountain system (the Himalayas), a plateau (Deccan plateau), large rivers (Ganges, Brahmaputra, and Indus), a delta (Ganges), a large plain (Indo-Gangetic), and offshore Islands, i.e., Sri Lanka and Maldives (https://geography.name/south-asia-landforms-and-resources/). The Himalayas constitutes the northern border, the Indian Ocean to the south, the Arabia Sea to the west, and the Bay of Bengal to the southeast of South Asia (Fig. 1). It has three major climatic zones, such as (i) a dry continental, subtropical climate (northern India and upland zone of Pakistan), (ii) equatorial climates (southern India and southwest Sri Lanka), and (iii) tropical climate (the rest of South Asia) (Xue and Yanai, 2005). Abundant precipitation occurs during monsoon (June–September), particularly in July with 350 mm (Clemens et al., 2021), while March to May becomes the warmest summer months (i.e., long dry season). Winter typically spans from November to February. The region has a diverse range of ecosystems and known as a hotspot of biodiversity (Hughes, 2017) with 63 ecoregions. It is worth mentioning that we excluded Maldives from our analyses, because islands that constitute Maldives are smaller than the spatial resolution of the MODIS datasets we used in this study.

2.2. Data used

We used three primary datasets in this study, such as (i) Terra/MODIS LST image, (ii) ecoregions of South Asia, and (iii) teleconnections. Monthly Terra MODIS acquired daytime and nighttime LST (MODIS/Terra Land Surface Temperature/Emissivity Monthly L3 Global 0.05 Deg CMG — MOD11C3 v061) images were downloaded from National Aeronautics and Space Administration's (NASA) Land Processes Distributed Active Archive Center (LP DAAC) in Hierarchical Data Format (HDF) with a spatial resolution of 5.6 km. The start and end dates of the images were from 01 February 2000 to 31 December 2021. We used the latest version (v061) of MOD11C3 product because it has improvement over the previous versions with an enhance accuracy of LST estimations via different changes in the calibration processes. It changed to the response versus scan angle approach, adjusted for the optical crosstalk in Terra MODIS infrared bands, corrected Terra MODIS forward look-up table, and polarization correction of the reflective solar bands.

The 63 ecoregions of South Asia were extracted from the global RESOLVE Ecoregions 2017 dataset consisting of 846 terrestrial ecoregions of our living planet Earth that represents the biological diversity of fauna and flora (Dinerstein et al., 2017). The dataset was introduced in 2001 to support the analyses of the global climate change influence on nature by ecologists towards the modern conservation planning for a sustainable global environment. Monthly anomalies of the atmospheric oscillation indices (teleconnections data) were retrieved from the NOAA's (National Oceanic and Atmospheric Administration) National Centers for Environmental Information— NCEI (NOAA, 2022) and Climate Prediction Center— CPC (NOAA/NWS, 2022) from 2000 to 2021. It was used to find any relationships of LST trends with the large-scale oscillations in South Asia.

2.3. Preparation of MODIS LST time series

From the downloaded MOD11C3 v061 data, four layers, i.e., daytime LST, quality Layer of daytime LST, nighttime LST, and quality layer of nighttime LST, were extracted to generate the monthly images and clipped them for South Asia. The LST layers in each image were multiplied by the scale factor of 0.02 to convert the LST values into Kelvin (K). The quality control layers in each image were used to determine the unqualified pixels and gaps resulted from the presences of cloud and aerosols during the time of acquisition. The pixels with LST average errors greater than or equal to three Kelvin (K) were excluded from the LST layers. The percentages of eliminated pixels for the day and nighttime images were insignificant, i.e., 0.059 and 0.077%, respectively. Finally, time-series of monthly and annual day and nighttime LSTs were prepared by stack-layering the monthly images with qualified pixels for the period 2000 to 2021.

2.4. Estimation of the pixel- and object-based LST trends

We followed two different approaches in estimating the trends from the day and nighttime LST time-series— pixel-based and object-based. The pixel-based approach was carried out over each pixel in the time-series for both monthly and annual. For the object-based approach, we estimated the average values of the monthly and annual day and nighttime LSTs in the time-series for each of the 63 ecoregions. In both approaches, we utilized two non-parametric statistical methods, such as Mann–Kendall (MK) test (Mann, 1945) and Sen's slope estimator (SSE) (Sen, 1968). MK analyzed difference in signs between observations, and SSE evaluated the magnitude and direction of the trends— warming or cooling. Through MK, we also determined the significance of the trends at 95 and 99% confidence levels.

MK test statistic S was calculated by the following equation (Eq. 1):

$$S = \sum_{k=1}^{n-1} \sum_{j=k+1}^{n} sgn(x_j - x_k) \tag{1}$$

where

$$sgn(x_j - x_k) = \begin{cases} +1 \text{ if } (x_j - x_k) \rangle 0 \\ 0 \text{ if } (x_j - x_k) = 0 \\ -1 \text{ if } (x_j - x_k) \langle 0 \end{cases} \tag{2}$$

n is the number of observations, and x_j and x_k are from $k = 1, 2, \ldots, n-1$ and $j = k + 1, \ldots, n$ in the LST time series. The mean of S is 0, and the variance of S is calculated as follows:

$$var(S) = \frac{n(n-1)(2n+5)}{18} \tag{3}$$

when $n > 10$, the standard normal test statistic Z is computed as follows:

$$Z = \begin{cases} \dfrac{S-1}{\sqrt{var(S)}} & \text{if } S > 0 \\ 0 \text{ if } S = 0 \\ \dfrac{S+1}{\sqrt{var(S)}} & \text{if } S < 0 \end{cases} \tag{4}$$

Positive and negative values of Z indicate increasing and decreasing trends, respectively.

The magnitudes of trends in LST time-series were calculated by Sen's slope estimator as follows (Eq. 5):

$$\beta = \text{Median}\left(\frac{x_j - x_i}{j - i}\right), j > i \tag{5}$$

where β is the Sen's slope for the set of pairs (i, x_i) in x_i time series with the elements (x_i, x_j) fulfilling $j > i$. The outcomes of $\beta > 0$ indicates upward trend (warming), otherwise downward trend (cooling) during the LST time-series.

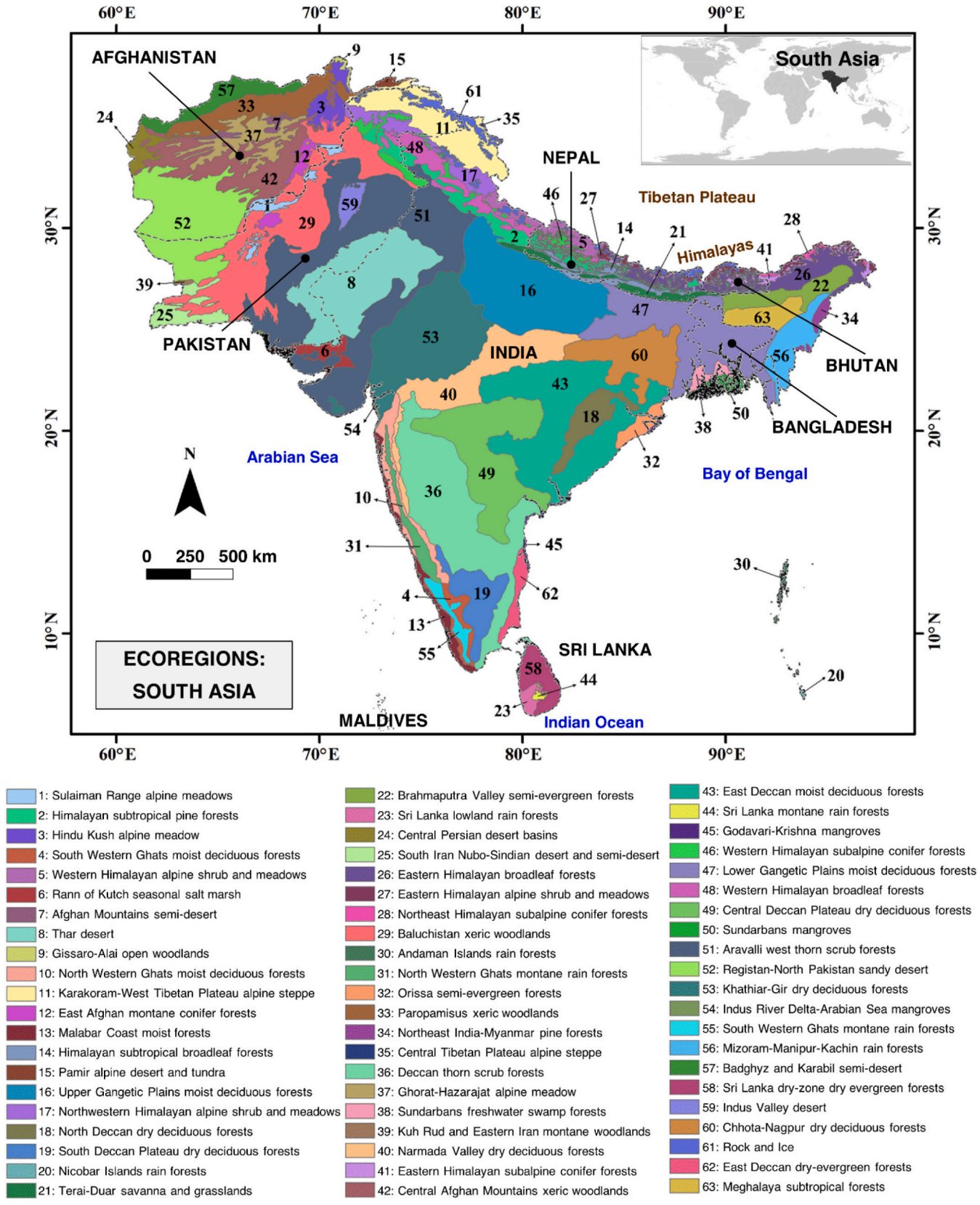

Fig. 1. Study area showing the ecoregions of South Asia.

2.5. Correlations of the atmospheric oscillation indices with LST trends

The atmospheric oscillations linked with south Asia climate were initially discussed in the introduction part. Moreover, in the following sentences, the definition of each index is introduced (NOAA), 2022). El Niño and the Southern Oscillation (I.e., ENSO) is a periodic swing in sea surface temperature (El Niño) and the air pressure of the superimposing atmosphere (Southern Oscillation) over the equatorial Pacific Ocean and it includes SST, SOI, and OLR. SST denotes the average ocean temperature in the upper few meters. SOI is a standardized index to estimate the large-scale fluctuations in sea-level pressure between the western and eastern tropical Pacific. Long periods of positive (negative) SOI values overlap with anomalously cold(warm) ocean waters over the eastern tropical Pacific distinctive of La Niña (El Niño) phases. OLR is measured via the NOAA Advanced Very High-Resolution Radiometer (AVHRR) polar satellite to estimate the energy radiated from the warmer earth surface to cooler space. Positive (Negative) OLRs are denotative of improved (suppressed) convection, and accordingly, less (more) cloud tops' coverage stands for La Niña (El Niño) phases. DMI indicates the anomalous east-west temperature gradient across the Indian Ocean. PDO is a reoccurring pattern of large-scale climatic variations due to the atmosphere and ocean interactions within the mid-latitude pacific basin that happens over multiple decades timescale (i.e., not seasons). The PDO extremes have either the positive (i.e., warm) phase or the negative (i.e., cold) phase, as described by anomalies in the ocean temperature at the northeast and tropical Pacific Ocean. AO is a pattern that fluctuates between the differences in atmospheric pressure in the polar and middle latitudes. During the positive phase, pressure differences are above average above the central Atlantic Ocean and below average over the arctic territories. In the negative phase, the circumstances are inverted. NAO is a periodic fluctuation in the atmospheric sea-level pressure between the Icelandic low-pressure system and the subtropical (Azores) high-pressure in the Atlantic Ocean. The pressure differences control the types of dominating winds.

Correlation analyses were carried out between the anomalies of monthly atmospheric oscillation indices (SST Nino3.4, SOI, OLR, DMI, PDO, AO, and NOA) and the estimated LST trends for monthly day and nighttime. It was calculated by Pearson's correlation coefficients (r) using the following equation (Eq. 6) (Deshmukh et al., 2022a, 2022b; Schober et al., 2018) with the significance at 95% confidence levels. It identified the impact of large-scale atmospheric circulations on the monthly temperature trends in South Asia.

$$r = \left[\frac{\sum_{i=1}^{n}(x_i - \bar{x})(y_i - \bar{y})}{\sqrt{\sum_{i=1}^{n}(x_i - \bar{x})^2}\ \sqrt{\sum_{i=1}^{n}(y_i - \bar{y})^2}} \right] \quad (6)$$

where n is the number of observations, and the values and mean values of x and y variables are (x_i and y_i) and ($\bar{x}$ and $\bar{y}$), respectively.

To assess the performance of the coefficient values, we adopted a commonly used classification scheme, such as unsatisfactory ($r \leq 0.4$), acceptable ($r = 0.40$ to 0.60), satisfactory ($r = 0.60$ to 0.70), good ($r = 0.70$ to 0.85), and very good ($r = 0.85$ to 1.00) (Hassan et al., 2021).

3. Results

3.1. LST trends in the ecoregions

3.1.1. Daytime trend

In general, more ecoregions in South Asia experienced both monthly and annual daytime cooling than warming during the period 2000–2021 at the statistically significant level with 95% (Fig. 2A) and 99% (Fig. 2B)

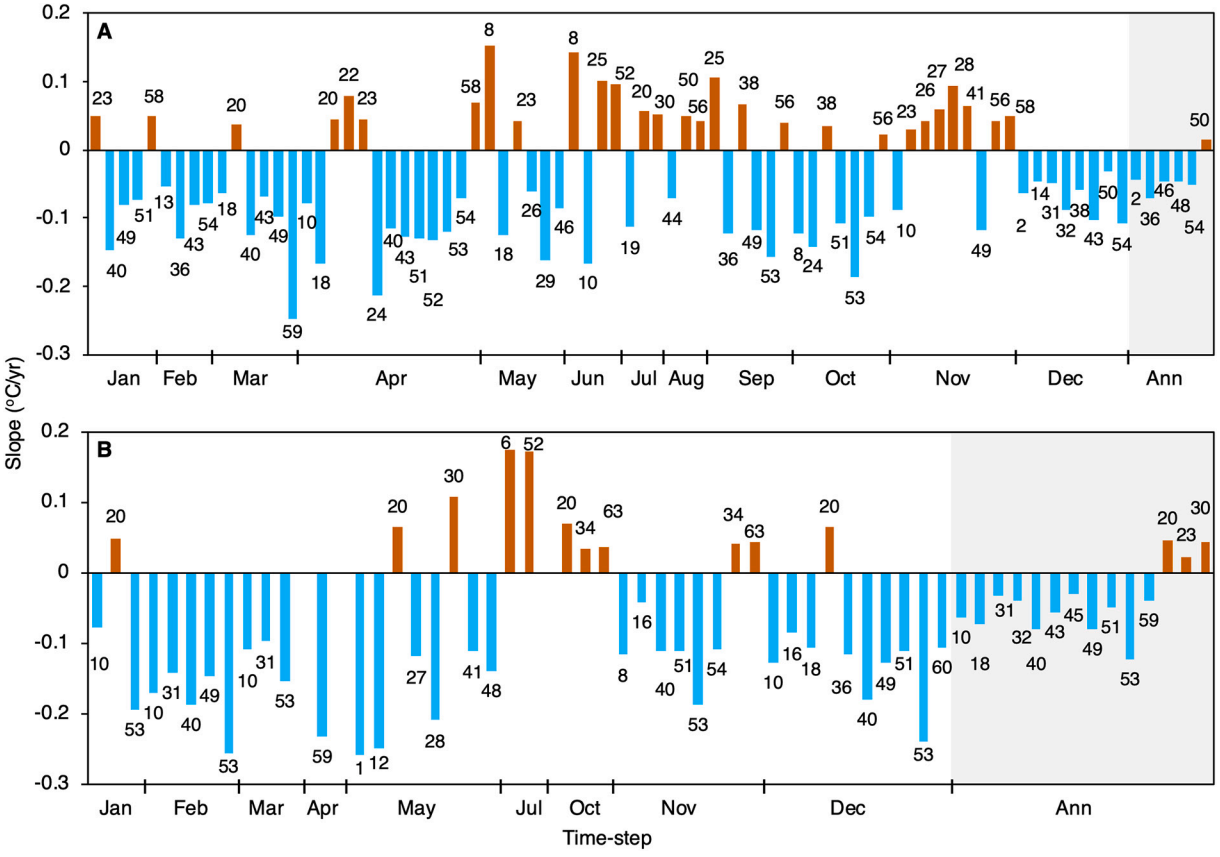

Fig. 2. Daytime cooling and warming trends in the ecoregions of South Asia. The confidence levels of the MK test and Sen slope estimator at 95% (**A**), and 99% (**B**). Time-step for months are January (Jan) to December (Dec), and the annual (Ann). Labels of the bars are the ecoregion number used in this study.

confidence. Twenty-five ecoregions showed monthly daytime cooling against fifteen warming ecoregions at the 95% confidence level, and nineteen ecoregions showed cooling against the six warming ecoregions at the 99% confidence level. At the 95% confidence, all months showed the daytime cooling at least in one ecoregion with the highest nine ecoregions in April, followed by eight ecoregions in December. February and June to October did not show any cooling ecoregion at the 99% confidence, where the highest nine ecoregions showed cooling in December. In contrast, January and March to November were warming at least in one ecoregion at the 95% confidence with the highest seven ecoregions in November. At the 99% confidence, warming was found in January, May, July, and October to December, where the highest in October for three ecoregions. Cooling was the highest in the ecoregion *59: Indus Valley desert* in March with the magnitudes of −0.25 °C/yr (95%) and − 0.26 °C/yr (99%), and the lowest in the *50: Sundarbans mangroves* in December with the magnitudes of −0.03 °C/yr (95%) and − 0.04 °C/yr (99%). Monthly daytime warming was the highest for the ecoregion *8: Thar desert* (0.15 °C/yr) in May and for the *6: Rann of Kutch seasonal salt marsh* in July with the magnitudes of 0.15 °C/yr (95%) and 0.18 °C/yr (99%), respectively. The lowest monthly daytime warming was observed in the ecoregions of *56: Mizoram-Manipur-Kachin rain forests* and *34: Northeast India-Myanmar pine forests* in October with the magnitudes of 0.02 °C/yr (95%) and 0.04 °C/yr (99%), respectively.

In the case of daytime annual trends, we identified five cooling ecoregions (i.e., 2: Himalayan subtropical pine forests, 36: Deccan thorn scrub forests, 46: Western Himalayan subalpine conifer forests, 48: Western Himalayan broadleaf forests, and 54: Indus River Delta-Arabian Sea mangroves) against one warming (50: Sundarbans mangroves) at the 95% confidence level (Fig. 2A). Also, 11 ecoregions (i.e., 10: North Western Ghats moist deciduous forests, 18: North Deccan dry deciduous forests, 31: North Western Ghats montane rain forests, 32: Orissa semi-evergreen forests, 40: Narmada Valley dry deciduous forests, 43: East Deccan moist deciduous forests, 45: Godavari-Krishna mangroves, 49: Central Deccan Plateau dry deciduous forests, 51: Aravalli west thorn scrub forests, 53: Khathiar-Gir dry deciduous forests, and 59: Indus Valley desert) showed cooling trends opposed to the three ecoregions (20: Nicobar Islands rain forests, 23: Sri Lanka lowland rain forests, and 30: Andaman Islands rain forests) with warming, at the 99% confidence level (Fig. 2B). The highest and lowest magnitudes of annual daytime cooling trend were − 0.07 and − 0.04 °C/yr for the ecoregions 36: Deccan thorn scrub forests and 2: Himalayan subtropical pine forests, respectively, at the 95% confidence level, and − 0.12 and − 0.03 °C/yr for 53: Khathiar-Gir dry deciduous forests and 45: Godavari-Krishna mangroves, respectively, at the 99% confidence level. On the contrary, the only annual warming ecoregion (50: Sundarbans mangroves) showed the magnitude of 0.01/yr °C at the 95% confidence, and the highest and lowest magnitudes at the 99% confidence were 0.05 and 0.02 °C/yr shown by the ecoregions 20: Nicobar Islands rain forests and 23: Sri Lanka lowland rain forests, respectively.

3.1.2. Nighttime trend

We did not find any monthly and annual nighttime cooling trend in the ecoregions of South Asia during the period 2000–2021 at the confidence levels of 95% (Fig. 3A and B) and 99% (Fig. 3C and D). The monthly warming magnitude was the maximum in *9: Gissaro-Alai open woodlands* in December and *53: Khathiar-Gir dry deciduous forests* ecoregions in July with the values of 0.19 and 0.16 °C/yr, and the minimum in *45: Godavari-Krishna mangroves* in September and *62: East Deccan dry-evergreen forests* in June with 0.02 and 0.04 °C/yr at the confidence levels of 95 and 99%, respectively. In the annual nighttime warming magnitude, *59: Indus Valley desert* (0.04 °C/yr at 95%) and *54: Indus River Delta-Arabian Sea mangroves* (0.06 °C/yr at 99%) ecoregions were the highest, and *60: Chhota-Nagpur dry deciduous forests* (0.02 °C/yr at 95%) and *47: Lower Gangetic Plains moist deciduous forests* (0.03 °C/yr at 99%) were the lowest.

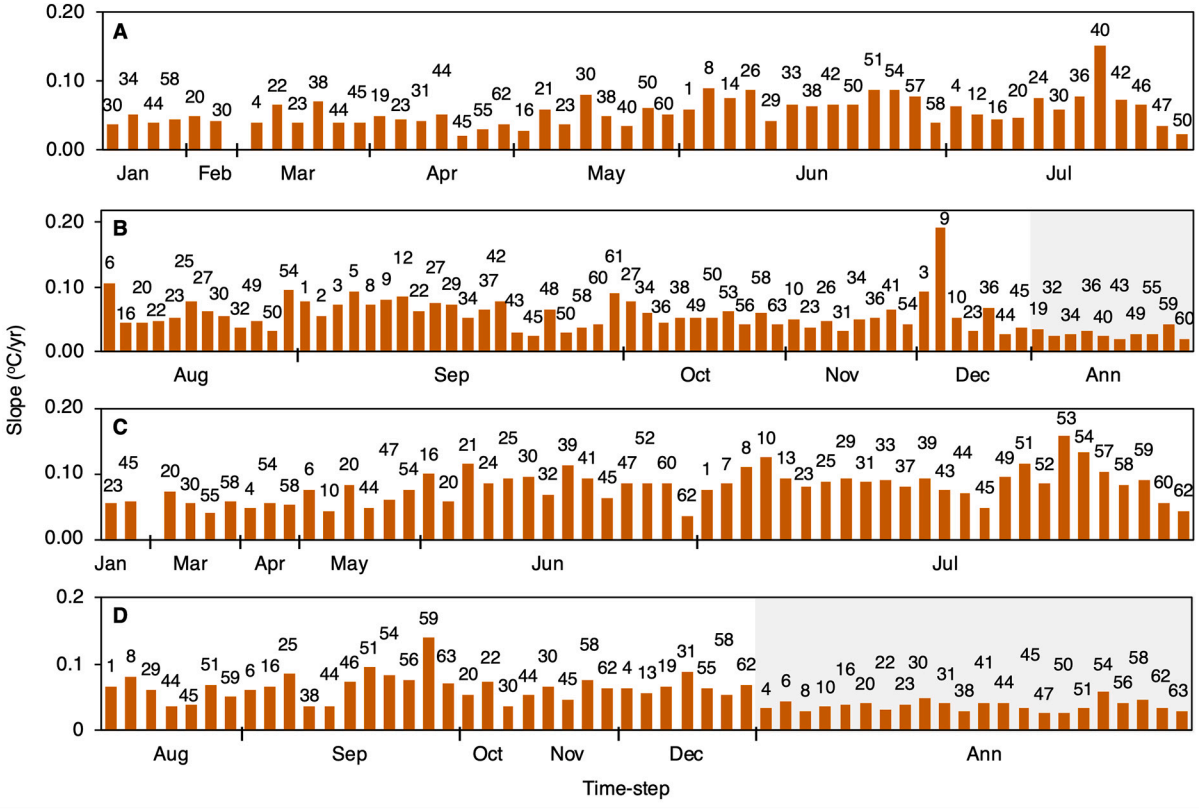

Fig. 3. Nighttime cooling and warming trends in the ecoregions of South Asia. The confidence levels of the MK test and Sen slope estimator at 95% (**A** and **B**), and 99% (**C** and **D**). Time-step for months are January (Jan) to December (Dec), and the annual (Ann). Labels of the bars are the ecoregion number used in this study.

3.2. Spatial trend

The spatial analysis (pixel based LST trends) exhibited significant trends (over 95% confidence level) during the daytime in December and annual (Table 1, and Fig. 4A and B), and nighttime in July, September and annual (Table 1, and Fig. 4C to E) in at least 30% area of South Asia. Daytime in November was also very close, where the significant trends were observed in 29.79% area (Table 1). The highest spatial coverage of significant trends (35.56% in Table 1) was found in the daytime of December, with the areas of 34.42% cooling and 1.14% warming. In December, daytime cooling was mostly prevailed in the central, central-west, and central-east regions of South Asia, with the higher magnitudes in the central-west (Fig. 4A). The most dominant and higher magnitude (≤ -0.3 °C/yr) of daytime cooling was in the *53: Khathiar-Gir dry deciduous forests* ecoregion in the west of South Asia, followed by *40: Narmada Valley dry deciduous forests* and south part of the *51: Aravalli west thorn scrub forests*. The northern parts of *36: Deccan thorn scrub forests* and *49: Central Deccan Plateau dry deciduous forests* ecoregions also showed moderate to higher daytime cooling (less than −0.11 °C/yr) in December, and the central-east ecoregions (e.g., *16: Upper Gangetic Plains moist deciduous forests*, *18: North Deccan dry deciduous forests*, *47: Lower Gangetic Plains moist deciduous forests*, and *60: Chhota-Nagpur dry deciduous forests*) represented moderate to low magnitudes (<0 to −0.20 °C/yr). Annually, the daytime cooling followed the similar spatial patterns of December, but with lower magnitudes. The exception was in the central-east with limited areas of cooling in *16: Upper Gangetic Plains moist deciduous forests* and *47: Lower Gangetic Plains moist deciduous forests*, and an additional daytime cooling was observed in *2: Himalayan subtropical pine forests* and the northern part of *51: Aravalli west thorn scrub forests*.

In July, the significant nighttime warming (over 95% confidence level) was demonstrated in the central-west, north central, and northwest of South Asia (Fig. 4C) with the higher magnitudes (>0.11 °C/yr) in the ecoregions of central-west (e.g., *51: Aravalli west thorn scrub forests;* northern parts of *8: Thar desert*, *38: Sundarbans freshwater swamp forests*, and *53: Khathiar-Gir dry deciduous forest;* western part of *49: Central Deccan Plateau dry deciduous forests*; and southern parts of *8: Thar desert*, *16: Upper Gangetic Plains moist deciduous forests*, *40: Narmada Valley dry deciduous forests*, and *53: Khathiar-Gir dry deciduous forest*). Moderate to low magnitudes of nighttime warming in July (>0 to 0.2 °C/yr) were observed in the north central and northwest ecoregions (e.g., *7: Afghan Mountains semi-desert*, *24: Central Persian desert basins*, *25: South Iran Nubo-Sindian desert and semi-desert*, *29: Baluchistan xeric woodlands*, *33: Paropamisus xeric woodlands*, *37: Ghorat-Hazarajat alpine meadow*, *42: Central Afghan Mountains xeric woodlands*, *51: Aravalli west thorn scrub forests*, *52: Registan-North Pakistan sandy desert*, *57: Badghyz and Karabil semi-desert*, and *59: Indus Valley desert*), and extreme southern island with the ecoregions of *23: Sri Lanka lowland rain forests*, *44: Sri Lanka montane rain forests* and *58: Sri Lanka dry-zone dry evergreen forests*. Nighttime in September (Fig. 3D) showed moderate to low warming (0 to 0.2 °C/yr) mostly in the ecoregions of North central (e.g., *8: Thar desert*, *16: Upper Gangetic Plains moist deciduous forests*, *29: Baluchistan xeric woodlands*, *37: Ghorat-Hazarajat alpine meadow*, *42: Central Afghan Mountains xeric woodlands*, *51: Aravalli west thorn scrub forests*, *59: Indus Valley desert*, and the northern parts of *2: Himalayan subtropical pine forests* and *43: East Deccan moist deciduous forests*), and some in the east (e.g., *63: Meghalaya subtropical forests*, northern part of *56: Mizoram-Manipur-Kachin rain forests*, and eastern part of *47: Lower Gangetic Plains moist deciduous forests*). Annual nighttime warming (Fig. 3E) was observed in low magnitude (>0 to 0.1 °C/yr) in the north-central (e.g., *8: Thar desert*, *16: Upper Gangetic Plains moist deciduous forests*, *25: South Iran Nubo-Sindian desert and semi-desert*, *51: Aravalli west thorn scrub forests*, and *59: Indus Valley desert*), south (e.g., *4: South Western Ghats moist deciduous forests*, *10: North Western Ghats moist deciduous forests*, *23: Sri Lanka lowland rain forests*, *31: North Western Ghats montane rain forests*, *44: Sri Lanka montane rain forests*, *45: Godavari-Krishna mangroves*, *55: South Western Ghats montane rain forests*, *58: Sri Lanka dry-zone dry evergreen forests* and *62: East Deccan dry-evergreen forests*, and scattered in *19: South Deccan Plateau dry deciduous forests*, *36: Deccan thorn scrub forests*, *43: East Deccan moist deciduous forests* and *49: Central Deccan Plateau dry deciduous forests*), and east (e.g., *56: Mizoram-Manipur-Kachin rain forests* and *63: Meghalaya subtropical forests*, and scattered in *22: Brahmaputra Valley semi-evergreen forests*, *26: Eastern Himalayan broadleaf forests*, *27: Eastern Himalayan alpine shrub and meadows*, *34: Northeast India-Myanmar pine forests*, *41: Eastern Himalayan subalpine conifer forests*, *47: Lower Gangetic Plains moist deciduous forests* and *60: Chhota-Nagpur dry deciduous forests*).

3.3. Correlation between LST trends and atmospheric oscillations

We presented the Pearson correlation coefficients (r) for daytime and nighttime in Fig. 5 and Fig. 6, respectively, in the ecoregions. During the daytime (Fig. 5), both positive and negative correlations were observed with values of 0.50 to 0.74 (acceptable to good) and − 0.50 to −0.73, respectively. Among the atmospheric indices, PDO showed positively correlated with 17 ecoregions in January (Fig. 5F), which was the highest in number for a single month. In contrast, negative correlations were found for 14 ecoregions (the highest number) with DMI in December (Fig. 5D), followed by 11 ecoregions with SST in November. Over the months of a year, PDO, SST, DMI and NAO exhibited the positive correlations with the highest number of ecoregions, i.e., 22, 21, 10 and 10, respectively, in compared to the negatively correlated AO, DMI, SST and OLR with 22, 21, 19 and 12 ecoregions, respectively. The least number of positive correlations was noticed for AO, OLR and SOI with 6, 5 and 4 ecoregions, respectively, and negative correlations of SOI, NAO and PDO with 9, 6 and 1 ecoregions, respectively.

During the nighttime (Fig. 6), positive and negative correlations were detected in the ecoregions with acceptable to good coefficient values ranged from 0.50 to 0.84 and − 0.50 to −0.71, respectively. The highest positive correlation was spotted for SST with 16 ecoregions in

Table 1
Cooling and warming areas in South Asia. Spatial coverage (area) is in percentage with the statistical confidence levels of 95% and 99% for both monthly (Jan to Dec) and annual time-steps.

LST	Trend	Confidence (%)	Area (%)												
			Jan	Feb	Mar	Apr	May	Jun	Jul	Aug	Sep	Oct	Nov	Dec	Annual
Daytime	Non-significant		84.07	76.95	81.23	80.05	79.93	89.55	90.04	91.16	83.54	79.10	70.21	64.44	67.26
	Cooling	95	7.73	9.25	9.50	11.61	7.82	2.55	1.29	3.32	7.27	10.87	10.71	12.99	11.36
		99	7.04	13.50	8.11	6.40	3.35	0.89	0.40	1.36	4.16	7.32	14.84	21.43	19.17
	Warming	95	0.80	0.22	0.82	1.39	6.09	4.95	4.85	3.15	3.29	1.87	2.64	0.99	1.34
		99	0.36	0.07	0.35	0.56	2.81	2.07	3.41	1.00	1.74	0.83	1.60	0.15	0.87
Nighttime	Non-significant		91.80	98.11	84.78	91.69	84.50	73.30	66.52	84.83	69.84	87.15	88.85	89.55	66.39
	Cooling	95	0.03	0.48	0.03	0.77	2.01	0.13	0.16	0.35	0.15	0.05	0.18	1.04	0.08
		99	0.00	0.08	0.01	0.12	0.24	0.01	0.02	0.05	0.02	0.01	0.04	0.11	0.03
	Warming	95	6.48	1.08	12.26	5.42	6.19	14.33	15.73	10.01	13.57	8.72	7.91	4.66	16.20
		99	1.70	0.26	2.91	2.00	7.06	12.23	17.58	4.77	16.42	4.07	3.02	4.64	17.29

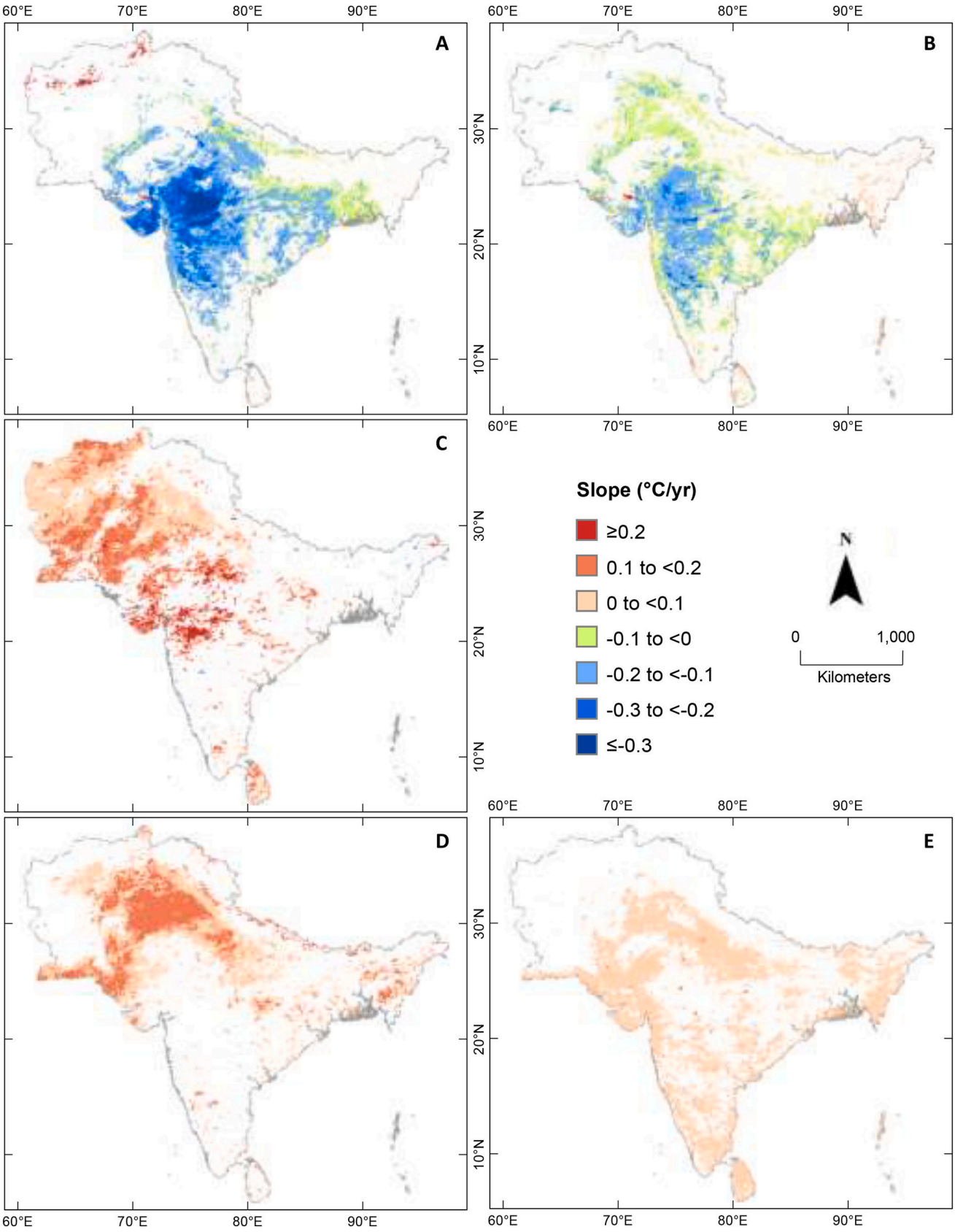

Fig. 4. Spatial dynamics of the cooling and warming in South Asia in different time-step, at least 95% confidence level. (**A**) daytime in December, (**B**) daytime at annual scale, (**C**) nighttime in July, (**D**) nighttime in September, and (**E**) nighttime at annual scale. This figure shows the time-step that demonstrated the trends for at least 30% of South Asia.

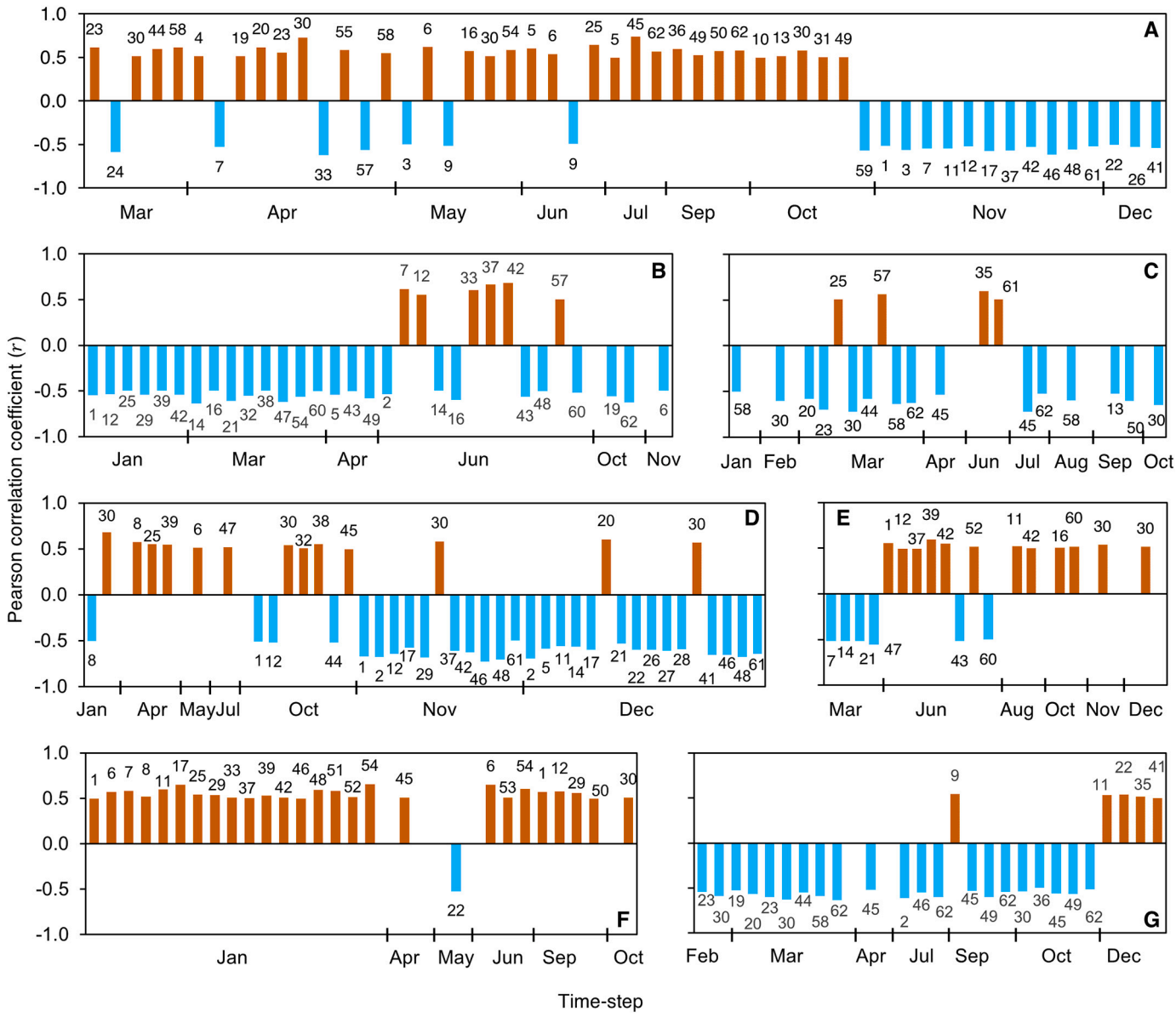

Fig. 5. Relationships of monthly daytime LSTs in the ecoregions with the large-scale atmospheric oscillations. The oscillation indices are: (**A**) SST, (**B**) AO, (**C**) SOI, (**D**) DMI, (**E**) NAO, (**F**) PDO, and (**G**) OLR, over 95% significance level.

April, followed by 14 ecoregions in January and March each (Fig. 6A). PDO also showed positive correlation with 13 ecoregions in January (Fig. 6F). In contrast, the highest negative correlation was observed for SOI with 13 ecoregions in January (Fig. 6C), followed by 11 ecoregions with AO in April (Fig. 6B) and OLR in March (Fig. 6G) each. Over the year, SST was positively correlated with the highest 38 ecoregions in compared to the highest negatively correlated SOI with 24 ecoregions. PDO, DMI and OLR were also found positively correlated with 25, 16 and 12 ecoregions, respectively, where NAO, SOI and AO were with the least number of ecoregions, i.e., 3, 3 and 1, respectively. On the contrary, OLR, NAO and AO were noticed for the negative correlations with 14, 13 and 13 ecoregions, respectively. While DMI and SST were negatively correlated with the least number of ecoregions (i.e., 8 and 3, respectively), we did not find any ecoregions that showed the negative correlation with PDO.

4. Discussion

4.1. Cooling and warming trends

The LST trend analysis of South Asia revealed that both warming and cooling trends occurred during 2000–2021, where most ecoregions (i.e., 34 out of the total 63) showed daytime cooling than warming. The most pronounced daytime cooling was observed in December (a dry month in the winter season) and nighttime warming in July and September (wet months in the monsoon season), where the magnitude of annual cooling was more than annual warming (Fig. 4). Most of the cooling ecoregions are having tropical forests that could be the reason of strong daytime cooling effects during the dry season (Li et al., 2015). Forests, with their deeper roots and high leaf area, move heat and moisture away from the ground into the atmosphere very efficiently during the daytime to cool the land surface faster. Releasing heat energy stored in forests during the day causes nighttime warming (Michiles and Gielow, 2008; Peng et al., 2014). Due to the larger heat capacity of forests, canopies stay warm at night by losing heat more slowly (Houspanossian et al., 2013). Stronger

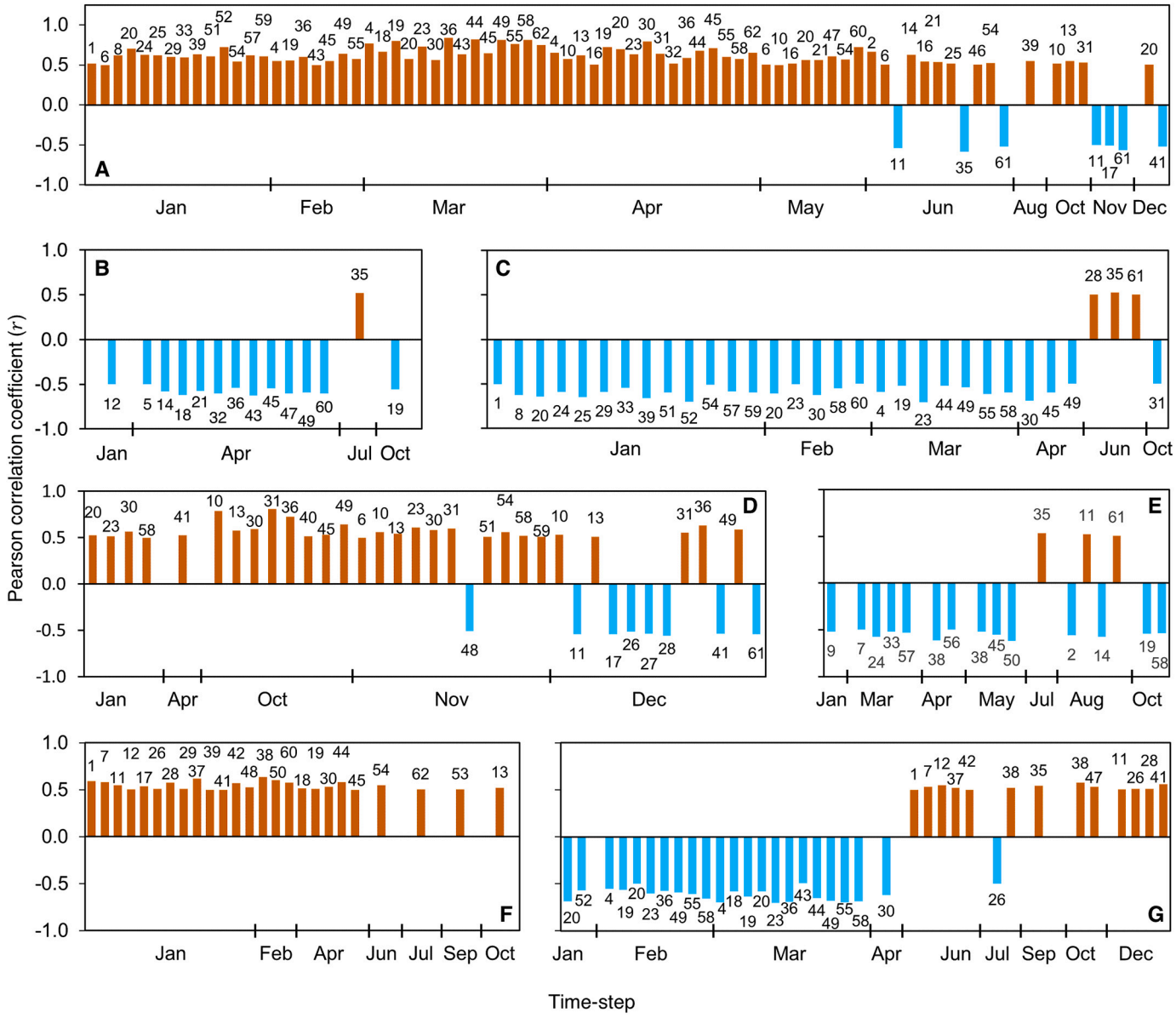

Fig. 6. Relationships of monthly nighttime LSTs in the ecoregions with the large-scale atmospheric oscillations. The oscillation indices are: (**A**) SST, (**B**) AO, (**C**) SOI, (**D**) DMI, (**E**) NAO, (**F**) PDO, and (**G**) OLR, over 95% significance level.

night warming occurs when forests receive more energy during daytime (Li et al., 2015), e.g., summer and monsoon seasons. Transpiration rate decreases with the increasing relative humidity of the air surrounding the forests (Krause et al., 2010). Therefore, the high moisture in the air during the monsoon season further slowdown the heat loss process of the ground through forests, especially at night. It could be a reason for receiving warming nighttime LST during the wet months of July and September in South Asia.

The temperature of the ground depends on the amount of incoming solar radiation and its interaction with the surface features. Literature indicated that the spatiotemporal local cooling and warming effects in the LST are mainly driven by the biophysical effects of evapotranspiration and albedo (Li et al., 2015). Albedo is the measure of the diffuse reflection part of the total incoming solar radiation that varies on different types of land surfaces, whereas evapotranspiration includes the combined process of evaporation from exposed soils/ground and transpiration through the vegetation. With the available water in the soil/ground, the evapotranspiration process cools the land surface escaping the water into the atmosphere (Food and Agriculture Organization of the United Nations (FAO), 2022). All these driving factors are controlled by different types of land cover (LC). Therefore, to understand the relationship of LST trends with different land cover types, we performed the Mann-Kendall test and Sen's Slope estimator on the time-series of each land cover area in the ecoregions during the study period. Here, we used the MODIS Land Cover Type Yearly data (MCD12Q1 v006 at 500 m) and IGBP (International Geosphere-Biosphere Programme) land cover classification system that defines ecosystems' surface classifications. The analysis showed that croplands (i.e., "Croplands" and "Cropland/natural vegetation mosaics" classes of IGBP) were a major LC type (i.e., >50% coverage in an ecoregion) in eight of the 11 ecoregions, where cooling trends were observed three and more times on a 13-unit scale (i.e., 12 months and annual) (Fig. 7). In general, all the cooling trends were noticed where the ecoregions had an increase in croplands, or an increase in other vegetation types like forests, shrublands, savannas, and grasslands.

The population has increased approximately 31% in the region over the last 20 years (from 1.42 billion in 2001 to 1.86 billion in 2020) (The World Bank, 2020). Agricultural products had increased remarkably in

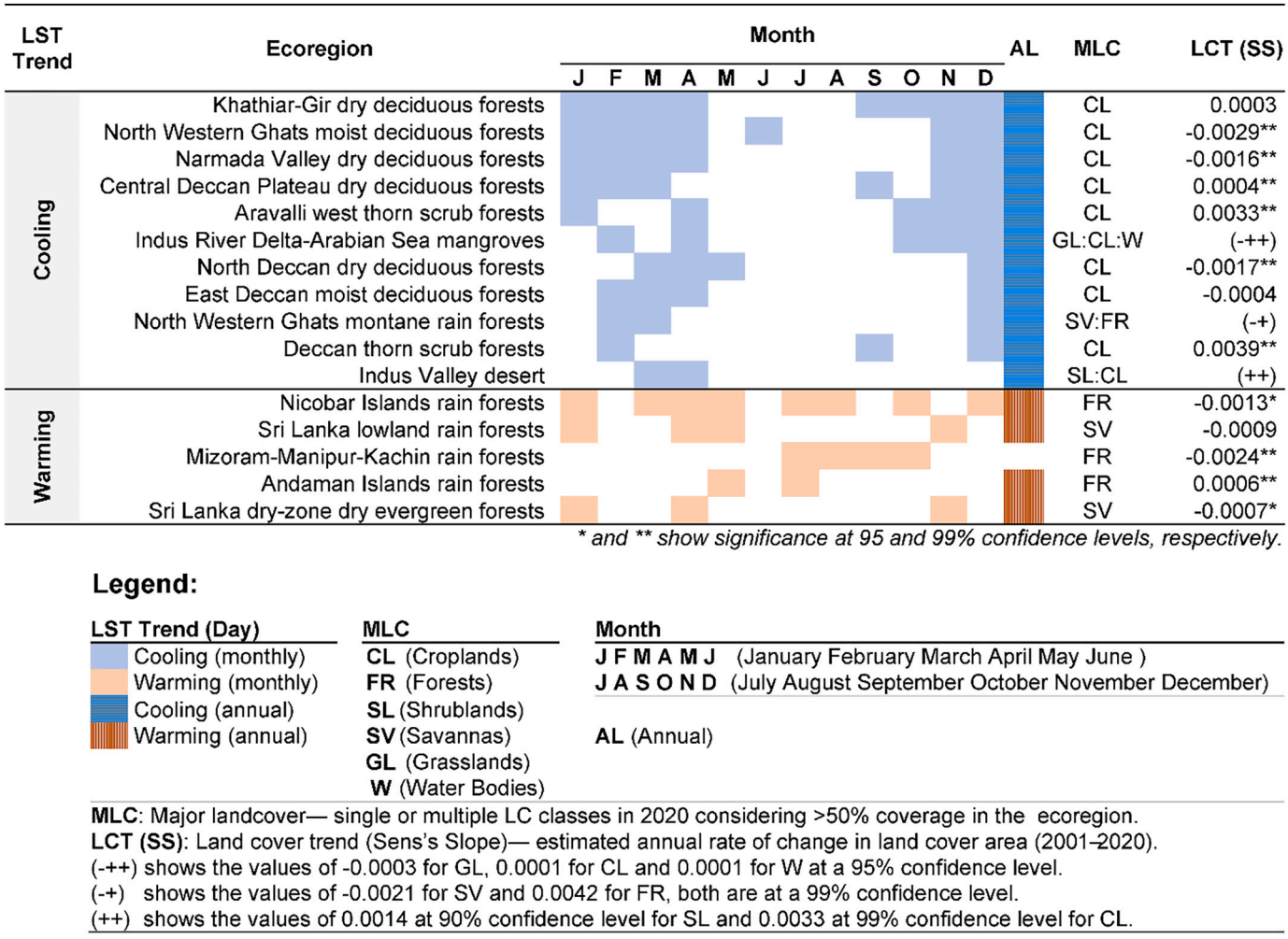

Fig. 7. Major land cover changing trend in the ecoregions that showed daytime cooling and warming (monthly and annual) during 2000–2021. Only those ecoregions were considered here that exhibited the frequency of three and more in a year.

the recent decades to secure the food demand for such a growing population (Alexandratos and Bruinsma, 2012). It was because of the yield growth, and thus agricultural growth, of major cereals resulting from new agricultural technologies and management measures (e.g., irrigation, pesticides, and fertilizers) (Wu et al., 2018), genetic improvement, expansion in arable land (to a very limited extent though), and increase in the cropping intensity (Morita, 2021). Water availability is a major factor in raising agricultural production, where the tropical climate in the region provides the best environmental conditions for achieving high yields (Morita, 2021). Besides, agricultural growth due to the increasing cropping intensity, i.e., multiple cropping in a year, in the new era of globalization (1990 onward) caused extensive irrigation expansion (Pingali, 2012). The expansion of land area equipped for irrigation, from 89 to 101 m ha from 2001 to 2019 (FAO (Food and Agriculture Organization of the United Nations), 2019)— calculated by combining the country values, caused such growth. Irrigated agriculture is around 40% of the total cultivated area in the region, the highest in the world (Hasanain et al., 2013), which had been expanding rapidly over the past few decades through the construction of canals and storage dams for surface water, and the exploitation of groundwater (Barker and Molle, 2004). As a matter of fact, part of the irrigation expansion in the region took place on arid and hyper-arid lands like the ecoregions of Thar desert and Indus Valley desert, which are not suitable for rain-fed agriculture.

In general, irrigation in the croplands is the most intensive during the dry period in the region that spans October/November through March/April. Coupled with the availability of water in the croplands through irrigation, the evapotranspiration process into the growing agricultural crops during the dry months accelerates land surface cooling (Ghafarian et al., 2022; Sun et al., 2016; Yang et al., 2020). In the evapotranspiration process, the evaporation fraction from cropped soil is the highest during the sowing stage of a field crop, and it decreases over the growing period as the crop develops. In contrast, transpiration becomes the main process from the matured to the harvest stages of the crop when canopy shades more and more of the ground area, i.e., high leaf area index (LAI) (Fig. 8). Therefore, the increasing trend of irrigated croplands in South Asia is probably the reason of the daytime cooling in most of the ecoregions during the dry months (Fig. 7). Matter of fact, we observed daytime cooling in an arid ecoregion, i.e., *59: Indus Valley desert*, because of the increasing area of irrigated croplands. It supports by another study that reported that a rise in the LAI caused an increase of the evaporation-driven cooling effect in the arid areas of the southern hemisphere (Forzieri et al., 2017). In contrast, the daytime warming we observed in five ecoregions (with frequency three and more in a year), four of those showed decreasing trends in vegetation (Fig. 7; MLC of Forests or Savannas). Here, vegetation decrease could be a reason of decreasing evapotranspiration process in the ecoregions to sufficiently lowering the LST. Besides, the ecoregion (*30: Andaman Islands rain forests*) showed warming trend most likely due to the presence of mature forests as a dominant coverage, which has the limited evapotranspiration capacity in compared to the young forests (Murakami et al., 2000). Interestingly, all five ecoregions prevail in the saline environment due to being close

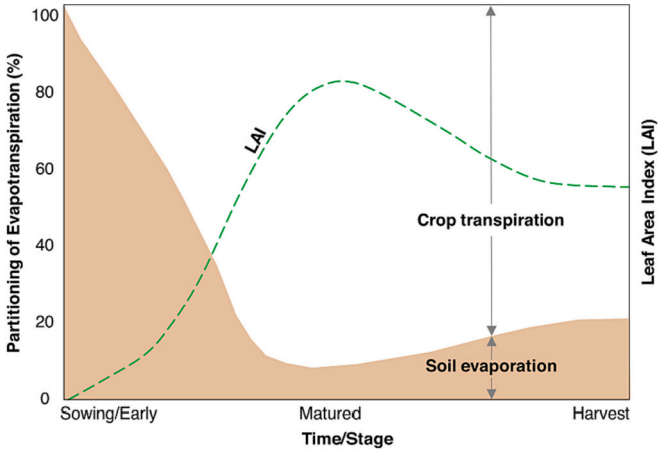

Fig. 8. Contribution of evaporation and transpiration in the evapotranspiration mechanism for an annual field crop over the growing period—modified from FAO.

by or surrounded ocean. It contributes to higher salinity in both soil and the atmosphere of the ecoregions which hinders the normal growth and evapotranspiration of the forests (Al-Busaidi and Yamamoto, 2011; Tomar and Gupta, 1985). Reducing evapotranspiration in the ecoregions could be another reason for daytime warming trends.

4.2. Influence of the atmospheric oscillations

In general, SST (ENSO: Niño 3.4) had the most significant influence on the LST in the ecoregions of South Asia during both day and night over the months for the period 2000—2021 (Figs. 5 and 6). It has the most positive influence from March to October during the day (Fig. 5A), and January to April during the night (Fig. 6A). Lack of the significant influence (negative correlation) of SST and DMI during the daytime in November and December, coupled with the positive influence of OLR in December, might be related to the cooling trends observed in the winter months. Other studies also indicated a greater impact of SST (ENSO: Niño 3.4) on faster decrease in temperature during cooling in winter in the area than increasing temperature for warming (Mallick et al., 2022b). The SST in South Asia comes as the easterly air from the Pacific Ocean (as Niño 3.4) and westerly from the tropical Indian Ocean (as DMI). The cold air from the Siberian High (circumpolar westerlies) approaches South Asia starting in October (Xue and Yanai, 2005). It develops a subtropical westerly jet stream at the northwestern end of the Himalayas that further intensify and extends southeastward causing winter circulation during November and December (Hamilton, 1974; Yeh et al., 1959). The circulation limited the easterly jet stream (including westerly) that might be a cause of negative correlations with the Niño 3.4 SST in November and December. Further, the Himalayas in the north, which is the southern periphery of the vast and high Tibetan Plateau, block the advancement of cold polar air from the north to go around than over it (Xue and Yanai, 2005). It forces the cool polar air coming through the northwest of the Himalayas. It, coupled with limited westerly SST (negative DMI) and positive OLR, might be a reason of more intense cooling trends observed in December in the central and west of South Asia (Fig. 4A) in compared to the northeast.

During the nighttime, we did not find any significant positive correlations of LST with SST (ENSO: Niño 3.4) in July and September, except with one ecoregion each for AO, NAO, PDO, and OLR in July, and PDO and OLR in September (Fig. 6). Tropical easterly jet in the summer season (continue through the monsoon) replaces the subtropical westerly jet of the winter season (Koteswaram, 1958). The high temperature during the summer over the Tibetan Plateau leads to the formation of the tropical easterly jet over South Asia. Easterly subtropical jet stream brings temperature (SST) and moisture from the Pacific Ocean during monsoon, and monsoon depressions in the Bay of Bengal occurs from June to September that reach the central parts before weakening (Xue and Yanai, 2005). The monsoon rainfall minimizes the temperature in the area, especially in the eastern and southeastern parts. With the less influence of the monsoon during that time in the west and northwest, coupled with the cloud coverage and lack of the SST influence in July and September, the diurnal cooling process hinders at nights (absence of the Sun). It might be a reason of the warming trends at the nighttime more pronounced in the west and northwest of South Asia, especially during July and September (Fig. 4). Although, PDO has greater positive correlations with LST in the earlier months of a year, i.e., days in January (Fig. 5F) and nights from January to April (Fig. 6F), it did not show any influence with cooling and warming trends in South Asia.

4.3. Ecological significance

The 63 ecoregions of South Asia are a repository of terrestrial, freshwater, terrestrial-coastal (e.g., mangroves and salt marshes) and marine habitats, including the three world's biodiversity hotspots of biologically rich land areas, i.e., the Himalayas, the tropical Indo-Burma, and the Western Ghats Mountain range and Sri Lanka (Saran, 2021). The forest ecosystems in the ecoregions cover 17% of South Asian land, and 2.2% of the world (FAO, 2020), constituting an extensive and valuable global carbon storage. The carbon storage is considered for the species richness (Strassburg et al., 2010), and some threatened species rely on carbon-rich habitats in the subtropical and tropical regions (Sheil et al., 2016), like South Asian forests. These forests are home to thousands of wildlife species (i.e., mammals, birds, reptiles, and amphibians), which play a significant role in the ecosystem functions like pollinators, seed dispersal, and pest control (Rajpar, 2018). The cooling or warming (climate change) observed in many ecoregions of South Asia would ultimately drive them to terrestrial biodiversity loss and affect carbon storage (Malhi et al., 2020). It may have negative impacts (directly or indirectly) on the inhabit, forage, perch, loaf, and breed for the survival and existence of the wildlife species in the ecoregions (Rajpar, 2018). The change (cooling/warming) of typical climate in the ecoregions due to land use change, such as cropland expansion and deforestation, would likely negatively impacting biodiversity and carbon storage in the biodiversity hotspots (Molotoks et al., 2020). The climate cooling/warming coupled with anthropogenic actions of land use change was apparent and likely to intensify over the coming decades (Hoffmann et al., 2019; Ohashi et al., 2019; Platts et al., 2019), resulting in habitat loss of wildlife species. Therefore, Therefore, it demands understanding ecological dynamics in the ecoregions due to the cooling/warming impacts and identify vulnerable hotspots. It would help to identify management interventions and formulate conservation and mitigation strategies that may assist biosphere resilience to such changes.

5. Conclusions

The spatiotemporal variations of LST in South Asia and its associated driving factors were demonstrated for 2000–2021. Estimated magnitudes and trends of LST showed warming and cooling, with daytime cooling in December and nighttime warming in July and September in most ecoregions. Significant daytime cooling was in the central, central-west and central-east ecoregions, and nighttime warming in the central-west, north-central, and northwest. The magnitudes of the annual cooling trends were more than the warming trends in the ecoregions. Land cover with the natural vegetation, irrigated agriculture, and atmospheric oscillations like PDO, SST, DMI and NAO exhibited positive correlations with the cooling trends and thus could be the main influential factors. This study contributes to a better understanding of temperature impacts on the ecoregions due to the ongoing climate change that would be useful for the policymaker to plan for sustainable development in South Asia concerning the excessive demands of food, water,

and energy supplies for the massive population growth. We strongly recommend a careful evaluation before adopting this study results for the region.

Funding

This study received partial funding from the Natural Sciences and Engineering Research Council of Canada — Discovery Grants program (NSERC DG) to Q. Hassan.

Authorship contributions

Mohamed Shawky: Conceptualization, Methodology, Data processing, Writing—original draft

M. Razu Ahmed: Conceptualization, Methodology, Data processing, Writing—original draft.

Ebrahim Ghaderpour: Conceptualization, Methodology, Data processing, Writing—review & editing.

Anil Gupta: Methodology, Writing—review & editing.

Gopal Achari: Methodology, Writing—review & editing.

Ashraf Dewan: Methodology, Writing—review & editing.

Quazi K. Hassan: Conceptualization, Methodology, Writing—review & editing, Funding acquisition, Supervision.

Declaration of Competing Interest

Authors declare that they have no competing interests.

Data availability

All the output data have been available in the main text in the form of figures and tables.

Acknowledgments

We would like to thank the anonymous reviewers for valuable feedback to improve the paper.

References

Ahmed, A.U., Hill, R.V., Smith, L.C., Wiesmann, D., Frankenberger, T.R., Gulati, K., Quabili, W., Yohannes, Y., 2007. The world's Most Deprived: Characteristics and Causes of Extreme Poverty and Hunger, 2020 Discussion Paper 43. Food Policy, January 2007. International Food Policy Research Institute (IFPRI), Washington, D. C.. https://doi.org/10.2499/0896297705

Ahmed, M.R., Hassan, Q.K., Abdollahi, M., Gupta, A., 2019a. Introducing a new remote sensing-based model for forecasting Forest fire danger conditions at a four-day scale. Remote Sens. 11, 2101. https://doi.org/10.3390/rs11182101.

Ahmed, K., Shahid, S., Wang, X., Nawaz, N., Khan, N., 2019b. Spatiotemporal changes in aridity of Pakistan during 1901-2016. Hydrol. Earth Syst. Sci. 23, 3081–3096. https://doi.org/10.5194/hess-23-3081-2019.

Akbar, T.A., Hassan, Q.K., Ishaq, S., Batool, M., Butt, H.J., Jabbar, H., 2019. Investigative spatial distribution and modelling of existing and future urban land changes and its impact on urbanization and economy. Remote Sens. 11, 105. https://doi.org/10.3390/rs11020105.

Al-Busaidi, A., Yamamoto, T., 2011. The impact of seawater salinity on evapotranspiration and plant growth under different meteorological conditions. In: Gerosa, Giacomo (Ed.), Evapotranspiration - from Measurements to Agricultural and Environmental Applications. InTech, Rijeka, Croatia, pp. 245–262.

Alexandratos, N., Bruinsma, J., 2012. World agriculture towards 2030/2050: The 2012 revision (No. No. 12-03). In: ESA Working Paper No. 12–03, ESA Working Paper. Rome.

Azad, S., Rajeevan, M., 2016. Possible shift in the ENSO-Indian monsoon rainfall relationship under future global warming. Sci. Rep. 6, 20145. https://doi.org/10.1038/srep20145.

Babel, M.S., Wahi, S.M., 2008. Freshwater Under Threat: South Asia, Vulnerability Assessment of Freshwater Resources to Environmental Change. Nairobi, Kenya.

Barker, Randolph, Molle, F., 2004. Evolution of irrigation in South and Southeast Asia (No. Research Report 5). In: Comprehensive Assessment of Water Management in Agriculture, Comprehensive assessment of water management in agriculture. Colombo, Sri Lanka.

Castellanos-Acuna, D., Hamann, A., 2020. A cross-checked global monthly weather station database for precipitation covering the period 1901–2010. Geosci. Data J. 7, 27–37. https://doi.org/10.1002/gdj3.88.

Charles, K., 2008. A picture of climate change in the Himalayas. Nat. https://doi.org/10.1038/news.2008.1055.

Clemens, S.C., Yamamoto, M., Thirumalai, K., Giosan, L., Richey, J.N., Nilsson-Kerr, K., Rosenthal, Y., Anand, P., McGrath, S.M., 2021. Remote and local drivers of pleistocene south Asian summer monsoon precipitation: a test for future predictions. Sci. Adv. 7, eabg3848. https://doi.org/10.1126/sciadv.abg3848.

Deshmukh, D., Ahmed, M.R., Dominic, J.A., Gupta, A., Achari, G., Hassan, Q.K., 2022a. Suitability assessment of weather networks for wind data measurements in the Athabasca Oil Sands area. Climate 10, 10. https://doi.org/10.3390/cli10020010.

Deshmukh, D., Ahmed, M.R., Dominic, J.A., Zaghloul, M.S., Gupta, A., Achari, G., Hassan, Q.K., 2022b. Quantifying relations and similarities of the meteorological parameters among the weather stations in the Alberta Oil Sands region. PLoS One 17, e0261610. https://doi.org/10.1371/journal.pone.0261610.

Dewan, A., Kiselev, G., Botje, D., Mahmud, G.I., Bhuian, M.H., Hassan, Q.K., 2021. Surface urban heat island intensity in five major cities of Bangladesh: patterns, drivers and trends. Sustain. Cities Soc. 71, 1–12. https://doi.org/10.1016/j.scs.2021.102926.

Di Cecco, G.J., Gouhier, T.C., 2018. Increased spatial and temporal autocorrelation of temperature under climate change. Sci. Rep. 8, 14850. https://doi.org/10.1038/s41598-018-33217-0.

Dinerstein, E., Olson, D., Joshi, A., et al., 2017. An ecoregion-based approach to protecting half the terrestrial realm. Bioscience 67, 534–545. https://doi.org/10.1093/BIOSCI/BIX014.

Eleftheriou, D., Kiachidis, K., Kalmintzis, G., Kalea, A., Bantasis, C., Koumadoraki, P., Spathara, M.E., Tsolaki, A., Tzampazidou, M.I., Gemitzi, A., 2018. Determination of annual and seasonal daytime and nighttime trends of MODIS LST over Greece - climate change implications. Sci. Total Environ. 616, 937–947. https://doi.org/10.1016/j.scitotenv.2017.10.226.

FAO (Food and Agriculture Organization of the United Nations), 2019. Land Use: Land Area Equipped for Irrigation [WWW Document]. FAOSTAT. URL. https://www.fao.org/faostat/en/#data/RL (accessed 5.5.22).

FAO (Food and Agriculture Organization of the United Nations), 2020. Global Forest Assessment Resources 2020: Main Report (Rome).

FAO (Food and Agriculture Organization of the United Nations), 2022. Chapter 1 - Introduction to Evapotranspiration [WWW Document]. Evapotranspiration Process, URL. https://www.fao.org/3/x0490e/x0490e01.jpg. accessed 5.7.22.

Forzieri, G., Alkama, R., Miralles, D.G., Cescatti, A., 2017. Satellites reveal contrasting responses of regional climate to the widespread greening of earth. Science 356, 1180–1184. https://doi.org/10.1126/science.aal1727.

Ghafarian, F., Wieland, R., Nendel, C., 2022. Estimating the evaporative cooling effect of irrigation within and above soybean canopy. Water (Switzerland) 14, 319. https://doi.org/10.3390/w14030319.

Gubler, S., Hunziker, S., Begert, M., Croci-Maspoli, M., Konzelmann, T., Brönnimann, S., Schwierz, C., Oria, C., Rosas, G., 2017. The influence of station density on climate data homogenization. Int. J. Climatol. 37, 4670–4683. https://doi.org/10.1002/joc.5114.

Hamilton, M.G., 1974. A satellite view of the south Asian summer monsoon. Weather 29, 82–95.

Hasanain, A., Ahmad, S., Zia Mehmood, M., Majeed, S., Zinabou, G., 2013. Irrigation and Water Use Efficiency in South Asia (No. Working Paper No. 68), GDN Working Paper Series. New Delhi.

Hassan, Q.K., Ejiagha, I.R., Ahmed, M.R., Gupta, A., Rangelova, E., Dewan, A., 2021. Remote sensing of local warming trend in Alberta, Canada during 2001–2020, and its relationship with large-scale atmospheric circulations. Remote Sens. 13, 1–21. https://doi.org/10.3390/rs13173441.

Hoffmann, S., Irl, S.D.H., Beierkuhnlein, C., 2019. Predicted climate shifts within terrestrial protected areas worldwide. Nat. Commun. 10, 1–10. https://doi.org/10.1038/s41467-019-12603-w.

Houspanossian, J., Nosetto, M., Jobbágy, E.G., 2013. Radiation budget changes with dry forest clearing in temperate Argentina. Glob. Chang. Biol. 19, 1211–1222. https://doi.org/10.1111/gcb.12121.

Hughes, A.C., 2017. Understanding the drivers of southeast Asian biodiversity loss. Ecosphere 8, e01624. https://doi.org/10.1002/ecs2.1624.

Intergovernmental Panel on Climate Change (IPCC), 2022. Documentation: About [WWW Document]. IPCC WGI Interact. Atlas Reg, Synth. URL. https://interactive-atlas.ipcc.ch/regional-information/about (accessed 5.19.22).

IPCC, 2018. Summary for policymakers. In: Masson-Delmotte, V., Zhai, P., Pörtner, H.-O., Roberts, D., Skea, J., Shukla, P.R., Piran, A., Moufouma-Okia, W., Péan, C., Pidcock, R., Connors, S., Matthews, J.B.R., Chen, Y., Zhou, X., Gomis, M.I., Lonnoy, E., Maycock, T., Tignor, M., Waterfield, T. (Eds.), Global Warming of 1.5°C. An IPCC Special Report on the Impacts of Global Warming of 1.5°C above Pre-Industrial Levels and Related Global Greenhouse Gas Emission Pathways, in the Context of Strengthening the Global Response to the Threat of Climate Change, pp. 3–24.

IPCC AR5, 2013. Climate Change 2013: The Physical Science Basis. Working Group I Contribution to the Fifth Assessment Report of the Intergovernmental Panel on Climate Change. Cambridge University Press, New York, USA. https://doi.org/10.1017/CBO9781107415324.

Iqbal, M.A., Penas, A., Cano-Ortiz, A., Kersebaum, K.C., Herrero, L., del Río, S., 2016. Analysis of recent changes in maximum and minimum temperatures in Pakistan. Atmos. Res. 168, 234–249. https://doi.org/10.1016/J.ATMOSRES.2015.09.016.

Islam, H.M.T., Islam, A.R.M.T., Abdullah-Al-Mahbub, M., Shahid, S., Tasnuva, A., Kamruzzaman, M., Hu, Z., Elbeltagi, A., Kabir, M.M., Salam, M.A., Ibrahim, S.M., 2021. Spatiotemporal changes and modulations of extreme climatic indices in monsoon-dominated climate region linkage with large-scale atmospheric oscillation. Atmos. Res. 264, 105840 https://doi.org/10.1016/J.ATMOSRES.2021.105840.

Jaber, S.M., Abu-Allaban, M.M., 2020. MODIS-based land surface temperature for climate variability and change research: the tale of a typical semi-arid to arid environment. Eur. J. Remote Sens. 53, 81–90. https://doi.org/10.1080/22797254.2020.1735264.

Jiang, S., Chen, X., Smettem, K., Wang, T., 2021. Climate and land use influences on changing spatiotemporal patterns of mountain vegetation cover in Southwest China. Ecol. Indic. 121, 107193 https://doi.org/10.1016/j.ecolind.2020.107193.

Koteswaram, P., 1958. The easterly jet stream in the tropics. Tellus. 10, 43–57.

Krause, G.H., Winter, K., Krause, B., Jahns, P., García, M., Aranda, J., Virgo, A., 2010. High-temperature tolerance of a tropical tree, Ficus insipida: methodological reassessment and climate change considerations. Funct. Plant Biol. 37, 890–900. https://doi.org/10.1071/FP10034.

Krishnamurthy, L., Krishnamurthy, V., 2013. Influence of PDO on South Asian summer monsoon and monsoon–ENSO relation. Clim. Dyn. 429 (42), 2397–2410. https://doi.org/10.1007/S00382-013-1856-Z.

Li, Y., Zhao, M., Motesharrei, S., Mu, Q., Kalnay, E., Li, S., 2015. Local cooling and warming effects of forests based on satellite observations. Nat. Commun. 6, 6603. https://doi.org/10.1038/ncomms7603.

Liu, J., Hagan, D.F.T., Liu, Y., 2020. Global land surface temperature change (2003–2017) and its relationship with climate drivers: AIRS, MODIS, and ERA5-land based analysis. Remote Sens. 13, 44. https://doi.org/10.3390/RS13010044.

Luintel, N., Ma, W., Ma, Y., Wang, B., Subba, S., 2019. Spatial and temporal variation of daytime and nighttime MODIS land surface temperature across Nepal. Atmos. Ocean. Sci. Lett. 12, 305–312. https://doi.org/10.1080/16742834.2019.1625701.

Malhi, Y., Franklin, J., Seddon, N., et al., 2020. Climate change and ecosystems: threats, opportunities and solutions. Philos Trans R Soc B Biol Sci 375. https://doi.org/10.1098/rstb.2019.0104.

Mallick, J., Islam, A.R.M.T., Ghose, B., Islam, H.M.T., Rana, Y., Hu, Z., Bhat, S.A., Pal, S. C., Ismail, Z. Bin, 2022a. Spatiotemporal trends of temperature extremes in Bangladesh under changing climate using multi-statistical techniques. Theor. Appl. Climatol. 147, 307–324. https://doi.org/10.1007/S00704-021-03828-1.

Mallick, J., Salam, R., Islam, H.M.T., Shahid, S., Kamruzzaman, M., Pal, S.C., Bhat, S.A., Elbeltagi, A., Rodrigues, T.R., Ibrahim, S.M., Islam, A.R.M.T., 2022b. Recent changes in temperature extremes in subtropical climate region and the role of large-scale atmospheric oscillation patterns. Theor. Appl. Climatol. 1481, 329–347. https://doi.org/10.1007/S00704-021-03914-4.

Mann, H.B., 1945. Nonparametric tests against trend. Econometrica 13, 245–259. https://doi.org/10.2307/1907187.

Mao, K.B., Ma, Y., Tan, X.L., Shen, X.Y., Liu, G., Li, Z.L., Chen, J.M., Xia, L., 2017. Global surface temperature change analysis based on MODIS data in recent twelve years. Adv. Sp. Res. 59, 503–512. https://doi.org/10.1016/J.ASR.2016.11.007.

Menne, M.J., Durre, I., Vose, R.S., Gleason, B.E., Houston, T.G., 2012. An overview of the global historical climatology network-daily database. J. Atmos. Ocean. Technol. 29, 897–910. https://doi.org/10.1175/JTECH-D-11-00103.1.

Michiles, A.A. Dos S., Gielow, R., 2008. Above-ground thermal energy storage rates, trunk heat fluxes and surface energy balance in a central Amazonian rainforest. Agric. For. Meteorol. 148, 917–930. https://doi.org/10.1016/j.agrformet.2008.01.001.

Midhuna, T.M., Dimri, A.P., 2019. Impact of arctic oscillation on Indian winter monsoon. Meteorog. Atmos. Phys. 131, 1157–1167. https://doi.org/10.1007/s00703-018-0628-z.

Molotoks, A., Henry, R., Stehfest, E., et al., 2020. Comparing the impact of future cropland expansion on global biodiversity and carbon storage across models and scenarios. Philos Trans R Soc B Biol Sci 375. https://doi.org/10.1098/rstb.2019.0189.

Mondal, A., Khare, D., Kundu, S., 2014. Spatial and temporal analysis of rainfall and temperature trend of India. Theor. Appl. Climatol. 122, 143–158. https://doi.org/10.1007/S00704-014-1283-Z.

Morita, 2021. Past growth in agricultural productivity in South Asia. In: Kumar, M.D. (Ed.), Current Directions in Water Scarcity Research. Elsevier Inc., pp. 137–156. https://doi.org/10.1016/b978-0-323-91277-8.00012-5

Murakami, S., Tsuboyama, Y., Shimizu, T., Fujieda, M., Noguchi, S., 2000. Variation of evapotranspiration with stand age and climate in a small Japanese forested catchment. J. Hydrol. 227, 114–127. https://doi.org/10.1016/S0022-1694(99)00175-4.

Nie, Y., Pritchard, H.D., Liu, Q., Hennig, T., Wang, W., Wang, X., Liu, S., Nepal, S., Samyn, D., Hewitt, K., Chen, X., 2021. Glacial change and hydrological implications in the Himalaya and Karakoram. Nat. Rev. Earth Environ. 2, 91–106. https://doi.org/10.1038/s43017-020-00124-w.

NOAA (National Oceanic and Atmospheric Administration), 2022. Climate Monitoring | National Centers for Environmental Information (NCEI). Retrieved December 23, 2022, from. https://www.ncei.noaa.gov/access/monitoring/products/.

NOAA (National Oceanic and Atmospheric Administration)/NWS (National Weather Service), 2022. CPC – Climate Weather Linkage: Teleconnections. Retrieved December 23, 2022, from. https://www.cpc.ncep.noaa.gov/products/precip/CWlink/daily_ao_index/teleconnections.shtml.

NourEldeen, N., Mao, K., Yuan, Z., Shen, X., Xu, T., Qin, Z., 2020. Analysis of the spatiotemporal change in land surface temperature for a long-term sequence in Africa (2003-2017). Remote Sens. 12, 1–24. https://doi.org/10.3390/rs12030488.

Ohashi, H., Hasegawa, T., Hirata, A., et al., 2019. Biodiversity can benefit from climate stabilization despite adverse side effects of land-based mitigation. Nat. Commun. 10, 1–11. https://doi.org/10.1038/s41467-019-13241-y.

Olivares-Contreras, V.A., Mattar, C., Gutiérrez, A.G., Jiménez, J.C., 2019. Warming trends in Patagonian subantartic forest. Int. J. Appl. Earth Obs. Geoinf. 76, 51–65. https://doi.org/10.1016/j.jag.2018.10.015.

Peng, S.S., Piao, S., Zeng, Z., Ciais, P., Zhou, L., Li, L.Z.X., Myneni, R.B., Yin, Y., Zeng, H., 2014. Afforestation in China cools local land surface temperature. Proc. Natl. Acad. Sci. U. S. A. 111, 2915–2919. https://doi.org/10.1073/pnas.1315126111.

Pepin, N., Bradley, R.S., Diaz, H.F., Baraer, M., Caceres, E.B., Forsythe, N., Fowler, H., Greenwood, G., Hashmi, M.Z., Liu, X.D., Miller, J.R., Ning, L., Ohmura, A., Palazzi, E., Rangwala, I., Schöner, W., Severskiy, I., Shahgedanova, M., Wang, M.B., Williamson, S.N., Yang, D.Q., 2015. Elevation-dependent warming in mountain regions of the world. Nat. Clim. Chang. 5, 424–430. https://doi.org/10.1038/nclimate2563.

Pingali, P.L., 2012. Green revolution: impacts, limits, andthe path ahead. Proc. Natl. Acad. Sci. U. S. A. 109, 12302–12308. https://doi.org/10.1073/pnas.0912953109.

Platts, P.J., Mason, S.C., Palmer, G., et al., 2019. Habitat availability explains variation in climate-driven range shifts across multiple taxonomic groups. Sci. Rep. 9, 1–10. https://doi.org/10.1038/s41598-019-51582-2.

Rahaman, K.R., Hassan, Q.K., Chowdhury, E.H., 2017. Quantification of local warming trend: a remote sensing-based approach. PLoS One 12, e0169423. https://doi.org/10.1371/journal.pone.0169423.

Rajpar, M.N., 2018. Tropical forests are an ideal habitat for wide Array of wildlife species. In: Sundarshana, P., Nageswara-Rao, M., Soneji, J. (Eds.), Tropical Forests, New Editio. Intech, London, UK, pp. 37–65.

Saran, S., 2021. South Asia needs a united voice at UN climate, biodiversity meetings. https://blogs.worldbank.org/endpovertyinsouthasia/south-asia-needs-united-voice-un-climate-biodiversity-meetings.

Schober, P., Boer, C., Schwarte, L.A., 2018. Correlation coefficients: appropriate use and interpretation. Anesth. Analg. 126, 1763–1768. https://doi.org/10.1213/ANE.0000000000002864.

Sen, P.K., 1968. Estimates of the regression coefficient based on Kendall's tau. J. Am. Stat. Assoc. 63, 1379–1389. https://doi.org/10.1080/01621459.1968.10480934.

Shahfahad Talukdar, S., Ali, R., Nguyen, K.-A., Naikoo, M.W., Liou, Y.-A., Islam, A.R.M. T., Mallick, J., Rahman, A., 2022. Monitoring drought pattern for pre- and post-monsoon seasons in a semi-arid region of western part of India. Environ. Monit. Assess. 194, 396. https://doi.org/10.1007/S10661-022-10028-5.

Sharma, K.P., 2012. Hydrology of South Asia from the perspective of global environmental changes. Hydro Nepal J. Water Energy Environ. 7–11. https://doi.org/10.3126/HN.V11I1.7196.

Sharma, S., Hamal, K., Khadka, N., Shrestha, D., Aryal, D., Thakuri, S., 2021. Drought characteristics over Nepal Himalaya and their relationship with climatic indices. Meteorol. Appl. 28, e1988 https://doi.org/10.1002/MET.1988.

Sheil, D., Ladd, B., Silva, L.C.R., et al., 2016. How are soil carbon and tropical biodiversity related? Environ. Conserv. 43, 231–241. https://doi.org/10.1017/S0376892916000011.

Strassburg, B.B.N., Kelly, A., Balmford, A., et al., 2010. Global congruence of carbon storage and biodiversity in terrestrial ecosystems. Conserv. Lett. 3, 98–105. https://doi.org/10.1111/j.1755-263X.2009.00092.x.

Sun, Z., Wang, Q., Batkhishig, O., Ouyang, Z., 2016. Relationship between evapotranspiration and land surface temperature under energy- and water-limited conditions in dry and cold climates. Adv. Meteorol. 2016, 1835487. https://doi.org/10.1155/2016/1835487.

Tan, J., Che, T., Wang, J., Liang, J., Zhang, Y., Ren, Z., 2021. Reconstruction of the daily modis land surface temperature product using the two-step improved similar pixels method. Remote Sens. 13, 1671. https://doi.org/10.3390/rs13091671.

Tepanosyan, G., Muradyan, V., Hovsepyan, A., Pinigin, G., Medvedev, A., Asmaryan, S., 2021. Studying spatial-temporal changes and relationship of land cover and surface urban Heat Island derived through remote sensing in Yerevan. Armenia. Build. Environ. 187, 107390 https://doi.org/10.1016/j.buildenv.2020.107390.

The World Bank, 2020. Population, Total - South Asia [WWW Document]. World Bank Open Data. https://data.worldbank.org/indicator/SP.POP.TOTL?end=2020&locations=8S&name_desc=false&start=2001 (accessed 4.28.22).

Tomar, O.S., Gupta, R.K., 1985. Performance of some forest tree species in saline soils under shallow and saline water-table conditions. Plant Soil 87, 329–335.

Wahiduzzaman, 2012. ENSO connection with monsoon rainfall over Bangladesh. Int. J. Appl. Sci. Eng. Res. 1, 26–38. https://doi.org/10.6088/IJASER.0020101003.

Wang, S.Y., Yoon, J.H., Gillies, R.R., Cho, C., 2013. What caused the Winter drought in Western Nepal during recent years? J. Clim. 26, 8241–8256. https://doi.org/10.1175/JCLI-D-12-00800.1.

Wu, W., Yu, Q., You, L., Chen, K., Tang, H., Liu, J., 2018. Global cropping intensity gaps: increasing food production without cropland expansion. Land Use Policy 76, 515–525. https://doi.org/10.1016/j.landusepol.2018.02.032.

Xue, Y., Yanai, M., 2005. Asia, climate of south. In: Oliver, J.E. (Ed.), Encyclopedia of World Climatology. Springer, Netherlands, Dordrecht, pp. 115–120. https://doi.org/10.1007/1-4020-3266-8_20.

Yan, Y., Mao, K., Shi, J., Piao, S., Shen, X., Dozier, J., Liu, Y., Ren, H.-L., Bao, Q., 2020. Driving forces of land surface temperature anomalous changes in North America in 2002–2018. Sci. Rep. 10, 1–13. https://doi.org/10.1038/s41598-020-63701-5.

Yang, Q., Huang, X., Tang, Q., 2020. Irrigation cooling effect on land surface temperature across China based on satellite observations. Sci. Total Environ. 705, 135984 https://doi.org/10.1016/j.scitotenv.2019.135984.

Yang, M., Zhao, W., Zhan, Q., Xiong, D., 2021. Spatiotemporal patterns of land surface temperature change in the Tibetan plateau based on MODIS/Terra daily product from 2000 to 2018. IEEE J Sel. Top. Appl. Earth Obs. Remote Sens. 14, 6501–6514. https://doi.org/10.1109/JSTARS.2021.3089851.

Yeh, T.C., Dao, S.Y., Li, M.T., 1959. The abrupt change of circulation over the northern hemisphere during June and October. Atmos. Sea Motion 249–267.

You, Q.L., Ren, G.Y., Zhang, Y.Q., Ren, Y.Y., Sun, X.B., Zhan, Y.J., Shrestha, A.B., Krishnan, R., 2017. An overview of studies of observed climate change in the Hindu

Kush Himalayan (HKH) region. Adv. Clim. Chang. Res. 8, 141–147. https://doi.org/10.1016/j.accre.2017.04.001.

Zhai, J., Mondal, S.K., Fischer, T., Wang, Y., Su, B., Huang, J., Tao, H., Wang, G., Ullah, W., Uddin, M.J., 2020. Future drought characteristics through a multi-model ensemble from CMIP6 over South Asia. Atmos. Res. 246, 105111 https://doi.org/10.1016/j.atmosres.2020.105111.

Zhao, W., Yang, M., Chang, R., Zhan, Q., Li, Z.-L., 2021. Surface warming trend analysis based on MODIS/Terra land surface temperature product at Gongga Mountain in the southeastern Tibetan plateau. J. Geophys. Res. Atmos. 126, 1–26. https://doi.org/10.1029/2020JD034205.